KINEMATIC AND MORPHOLOGICAL EVOLUTION AND DYNAMICS OF CORONAL MASS EJECTIONS IN THE INTERPLANETARY SPACE

by

Watanachak Poomvises
A Thesis proposal
Submitted to the
Graduate Faculty
of
George Mason University
In Partial fulfillment of
The Requirements for the Degree
of
Doctor of Philosophy
(Discipline)

Committee:

_____ Dr.Jie Zhang, Thesis proposal Director

_____ Dr.John Wallin, Committee Member

_____ Dr.Meraph Opher, Committee Member

_____ Dr.Arthur Poland, Committee Member

_____ Dr.Danial Carr, Committee Member

_____ Department Head, Department Chair

Date: _____ Semester Year
George Mason University
Fairfax, VA

Kinematic and Morphological Evolution and Dynamics of Coronal Mass Ejections in the Interplanetary Space

A thesis proposal submitted in partial fulfillment of the requirements for the degree of Doctor of Philosophy at George Mason University

By

Watanachak Poomvises
Civil and Environmental Engineering
George Washington University, Washington DC, 2002
Electronics Engineering
Assumption University, Thailand, 1999

Director: Dr.Jie Zhang, Professor
Department of Computational and Data Science

Semester Year
George Mason University
Fairfax, VA

Table of Contents

List of Tables

List of Figures

Abstract

KINEMATIC AND MORPHOLOGICAL EVOLUTION AND DYNAMICS OF CORONAL MASS EJECTIONS IN THE INTERPLANETARY SPACE

Watanachak Poomvises, PhD

George Mason University, Year

Thesis proposal Director: Dr.Jie Zhang

Coronal mass ejections (CMEs) are the main driver of the space weather, which describes the plasma, magnetic and particle conditions in space that affect Earth and its technological systems. The objective of this dissertation is to study the kinematics and morphological evolution of CMEs in the interplanetary space. First, I will make use of the latest STEREO (Solar TErrestrial RElations Observatory)/SECCHI (Sun Earth Connection Coronal and Heliospheric Investigation) observation to track a set of well observed CMEs for their evolution from the Sun to a large distance into the heliosphere. The kinematical parameters obtained are CME location, propagation velocity, and acceleration. The morhorlogical parameters are its size and expansion. Second, I will develop a theoretical model to explain the observed evolution of the CME, considering all the forces involved, including Lorentz force (for both propelling and constraining), thermal pressure force, gravity force and solar wind dragging force. The theoretical work will start from the test of the existing highly idealized CME evolution models, including flux rope model and the Melon-Seeds-Overpressure-expansion(MSOE) model. However, with the improved knowledge of the observations, I believe that a more comprehensive and practical model can be developed.

Chapter 1: Introduction

Space weather is about the varying physical conditions, concerning the states of plasma, magnetic fields, particles, and radiation, in the vast space beyond the Earths lower atmosphere. In addition to the space close to the Earth, it also embraces the interplanetary space and extends to the Suns atmosphere. It is now well known that the major driver of space weather is coronal mass ejection (CME), which originates in the Suns inner corona. When a CME propagates through the interplanetary space (called ICME) and happens to pass through the Earth's orbit, the CME may transfer a large amount of energy into the Earth's magnetosphere and cause a geomagnetic storm. Another space weather effect of CMEs is the so-called solar energetic particle (SEP) event, which may cause damage in electronic circuits in spacecraft and pose hazards to astronauts. Therefore, the study of CMEs is important from both scientific and practical points of views. The purpose of this dissertation is to study both kinematical and morphological evolutions of CMEs from observations, and understand the dynamical processes of CMEs using theoretical model.

CMEs are routinely observed by white light coronagraphs. Solar and Heliospheric Observatory (SOHO), launched on December 2, 1995 from the Kennedy Space Flight Center, Cape Canaveral, Florida, carried the Large Angle and Spectrometric Coronagraph (LASCO) instrument. Composing of a set of three coronagraphs that show obtain of solar corona from 1.1 to 32 Rs. LASCO has observed more than $10,000$ CMEs. LASCO data have been extensively used to study the initiation and propagation of CMEs. However, one limitation of CME study from SOHO/LASCO is that the speed measured is not the actual speed; it is the projected speed or measured from the plane-of-sky. STEREO (Solar TErrestrial RElations Observatory), designed to make much better observations of CMEs, was launched on 26 October, 2006. The STEREO consists of two identical satellites, one ahead and the

other behind the Earth along their orbits on the ecliptic plane. [Figure 1]

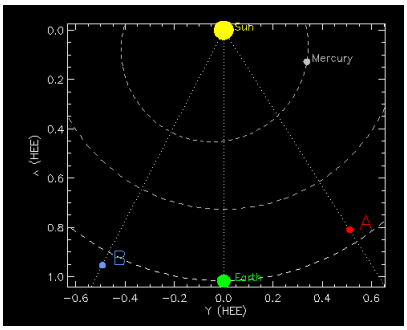

Figure 1.1: Positions of STEREO satellite A and B(*small red and blue circles*), sun (*yellow circle*) and earth (*green circle*)

The SECCHI instrument suite on STEREO has five complementing instruments: EUVI (Extreme Ultra Violet Imager), COR1 (Inner Coronagraph), COR2 (Outer Coronagraph), HI 1(Heliospheric Imager 1) and HI 2(Heliospheric Imager 2). The COR 1 is able to take images of the solar corona from 1.5-4.0 R_s. On the other hand, the COR 2 can take images of the solar corona from 3-15 R_s and HI 1 gives the field of view of the solar corona from 12-84 Rs.

Apparently, the STEREO/SECCHI is more advanced than SOHO/LASCO in term of studying CME evolutions. It has a much larger field of view, providing us more complete observations of CMEs propagation and expansion. Moreover, we can infer the information in 3-D space: 3-D position, 3D velocity, and 3-D acceleration, from the two data sets of STEREO/SECCHI from two advantage points in the heliosphere.

At present, most studies of CMEs/ICMEs are limited to the two ends: CMEs near the Sun and ICMEs near the Earth, leaving the evolution through the vast interplanetary space unknown. My research work will attack the CME evolution in the interplanetary space with the aid of STEREO observations. This study is important and also timely. In the following two sections, I will briefly summarize the current observational results on CMEs/ICMEs and the existing theoretical models of ICME evolution respectively. My existing research work related to the thesis topic is summarized in section 4. A detailed research plan will

be given in section 5 and 6.

Chapter 2: Current understanding on CME-ICME connections

Based on coronagraph observations near the Sun, the morphology of CMEs is often found to consist of three parts: a bright leading front followed by a dark cavity, and a brightness core in the cavity. The leading front is caused by compression and pile-up of ambient plasma following the CME initiation. The dark cavity is caused by the rapid expansion of the coherent CME magnetic structure, presumably a 3-D flux rope. At the near-Earth space, the cavity corresponds to the well known magnetic cloud structure seen in ICMEs. About one third of ICMEs have well-defined magnetic cloud structure. The plasma compression in the leading front may evolve into an interplanetary shock, as often observed in-situ as an abrupt change of plasma temperature and density.

Before the STEREO era, continuous tracking of individual CMEs throughout the heliosphere is not possible. However, several statistical studies of a large number of ICMEs, each of which are observed in-situ provide clues on possible CME evolution. On the kinematic evolution of CMEs between the Sun and the Earth, Gopalswamy et al (2000) [7] found a correlation between CME velocity at the Sun (projected velocity from LASCO)and the velocity of the counterpart ICMEs at 1 AU. The empirical formula of the inferred acceleration between the Sun and the Earth is described as

$$a(m/s^2) = 1.41 - 0.0035 * u(km/s) \tag{2.1}$$

where a in unit of m/s^2 and u represents the CME velocity in unit of km/s^2. This result was supported by Reiner et al (2003)[14], who measured deceleration of fast CMEs between the sun and the Earth using both radio and white light observations.

Liu et al (2005)[11] studied properties of ICMEs from 0.3 to 5.4 AU using in-situ data

from Helio 1 and 2, Advance Composition Explorer (ACE), WIND, and Ulysses. The data from Helio 1 and 2 had been used for the heliocentric distance from 0.3 to 1 AU since Decemeber 1974 to 1985. WIND and ACE, launched in 1994 and 1997 respectively, provided the measurement of solar wind in near-Earth space. Ulysses, launched in 1991, provided the data of solar wind from 1 to 5.4 AU. To identifying ICMEs in the solar wind data, Liu et al (2005)[11] utilized a set of signatures including low proton temperature and low alpha to proton density ratio $\frac{N_\alpha}{N_p} \geq 0.08$. They also used the ratio of proton temperature and the expected temperature of undisturbed solar wind $\frac{T_p}{T_{exp}}$, which may indicate the presence of ICMEs when this ratio is ≤ 0.5.. The expectation temperature is calculated as follows ([1] ,[12])

$$T_{exp} = \begin{cases} \frac{(0.016v-0.278)^3}{R} & v < 500\ kms^{-1}, \\ \frac{(0.77v-265)}{R} & v \geq 500\ kms^{-1}, \end{cases} \tag{2.2}$$

Based on these ICMEs, Liu et al (2005)[11] found the statistical dependence of ICME density $N(R)$,, velocity $V(R)$, temperature $T(R)$ and magnetic field on the distance R:

$$N(R) = (6.16 \pm 6.27) * R^{-2.32\pm0.07}(cm^{-3}) \tag{2.3}$$

$$v(R) = (458.40 \pm 6.27) * R^{-0.002\pm0.02}(kms^{-1}) \tag{2.4}$$

$$T(R) = (35401.1 \pm 1328.3) * R^{-0.32\pm0.06}(K) \tag{2.5}$$

$$B(R) = (7.35 \pm 0.40) * R^{-1.40\pm0.08}(nT) \tag{2.6}$$

The important results were that plasma density and magnetic field strength inside ICMEs decrease faster than the ambient solar wind but the temperature decreases slower than that in the solar wind.

Further, the physical properties within ICMEs are probably inter-related. Gonzalez et al (1998)found a correlation between maximum magnetic field strength ($|B_{max}|$) and maximum velocity V_{max}, which can be described as

$$|B_{max}|(nT) = 0.047V_{max}(km/s) - 1.1 \tag{2.7}$$

Owen and Cargill (2005)[13] found a similar correlation for magnetic field greater than $18nT$,

$$|B_{max}|(nT) = 0.047V_{max}(km/s) + 0.6 \tag{2.8}$$

There is also a possible relationship between CME bulk propagation speed, or cruise speed (i.e. speed at the center of mass, or at the centroid of the CME structure) and the structural expansion speed (i.e. how fast the CME front is moving away from the centroid). Owen et al (2005) [13] worked on a set of ICMEs whose starting time and ending time were identified by Richardson and Cane (2003) [17] They obtained the cruise speed V_{CR}, radial speeds at the leading edge V_{LE} of ICMEs and the trailing edge of ICMEs (V_{TE}). The expansion speed could be then inferred as $V_{EXP} = (V_{LE} - V_{TE})/2$. They found that leading edge velocity V_{LE} was a function of cruise velocity V_{CR}. They showed the relation between leading edge velocity V_{LE} and cruise velocity V_{CR} is

$$V_{LE}(km/s) = (1.30V_{CR} - 57.7)km/s \tag{2.9}$$

In short, existing studies provide useful but limited knowledge on CME evolution in the interplanetary space. Many important questions, from both scientific and practical point of views, remain unanswered. How does a CME change its velocity enroute to the Earth? Apparently, the assumption of a constant acceleration is an over-simplification, yielding poor

results in predicting the arrival time of ICME at 1 AU; this issue is practically important in forecasting space weather. How does a CME expand while it propagates through the interplanetary space? A good understanding on this issue helps predict the possibility of a CME impacting the Earth. How do the physical states of a CME evolve with time, such as internal magnetic field, density, temperature and pressure? In this thesis, I propose to solve these problems through both observational and theoretical means. In the next section, the existing CME evolution models are introduced.

Chapter 3: Existing theoretical models of CME propagation

In this section, I review two existing CME evolution models, one is the flux rope model by Chen(1996) [**?**] and other is MSOE model by Sisco [18]. One existing model, on the kinematical and morphological evolution of CMEs, is the so-call flux rope model[**?**], which also addresses CMEs initiation and propagation model. The model assumes a torus-geometry. The torus major radius, apex height, distance between the two footpoints are related as

$$R(t) = \frac{Z^2 + \frac{S_f^2}{4}}{2Z(t)} \tag{3.1}$$

In the model, the net force acting on the major radius can be derived as

$$F_R = \frac{I_t}{C^2 R}[ln(\frac{8R}{a}) + \frac{1}{2}\beta_p - \frac{1}{2}\frac{B_t^2}{B_{pa}^2} + 2\frac{R}{a}\frac{B_s}{B_{pa}} - 1 + \frac{\xi_i}{2}] + F_g + F_d \tag{3.2}$$

B_t the toroidal field component, $B_{pa} = B_p(a)$ the poloidal field component on the surface of the torus, B_s the external magnetic field which is perpendicular to the toroidal field, and $\xi_i = 2\int \frac{rB_p^2(r)dr}{a^2 B_{pa}^2}$ is the internal inductance. Part of internal inductance related with current distribution. $\beta_p = 8\pi(\bar{P} - P_a)/B_{pa}^2$, where $\bar{P}$ is the average pressure inside the flux rope,P_a is the ambient coronal pressure.

The gravitational force per unit length is given by

$$F_g = \pi a^2 m_i g(Z)(n_a - \bar{n}_T) \tag{3.3}$$

Where m_i is the ion mass, and na is the ambient solar wind density. $\bar{n}_T = \bar{n}_c + \bar{n}_p$ is

the total density of the loop and subscript c refers to cavity material and p to prominence material. Since the temperature of prominence is less than the temperature of the cavity $T_p << T_c$. The thermal pressure is calculated by $\bar{p} = 2\bar{n}_c k\bar{T}_c$. Within the flux rope the equation of state is given by

$$\frac{d}{dt}\left(\frac{\bar{p}}{\bar{\rho}^{\gamma}}\right) = 0 \tag{3.4}$$

Then the average mass density within the flux rope is given by $\bar{\rho} = \bar{n}_c m_i$, and γ is the polytropic index $1 \leq \gamma \leq \frac{5}{3}$. One of issues I would like to investigates is how the γ index possibly changes with distance. Chen (1996) used a constant value of 1.2 which is an assertion that the parallel thermal conductivity is high. The equation for pressure becomes

$$\bar{p} = C_{\gamma}\bar{\rho}^{\gamma} \tag{3.5}$$

Where the constant C_{γ} is found with the initial equilibrium values and is equal to

$$C_{\gamma} = \frac{2k\bar{T}_c}{\bar{n}_c^{\gamma-1} m_i} \tag{3.6}$$

where m_i is the ion mass, and k the Boltzmann constant. The total gravitational acceleration is given by

$$g(Z) = \frac{g_s}{1 + \frac{Z}{R_{\oplus}}^2} \tag{3.7}$$

Where $g_s = 2.74 * 10^4 cm/s^2$ and $R_{\oplus} = 6.96 * 10^5 km$ the solar radius. Z is apex height above photosphere. Another force is the drag force F_d which is given by

$$F_d = c_d n_a m_i a \mid V_a - V \mid\mid V_a - V \mid \tag{3.8}$$

where c_d is the drag coefficient. V_a is the ambient solar wind speed. $V \equiv \frac{dz}{dt}$ is the apex speed. Drag force and its variation with distance is one of the main issues in this thesis.

The expansion of the flux rope is described by the forces acting on the minor radius, a, which is

$$F_a = M\frac{dw}{dt} = \frac{I_t}{c^2 a}\left(\frac{B_t^2}{B_{pa}^2} - 1 + \beta_p\right) \tag{3.9}$$

Where w is the rate of expansion or minor radial expand speed $\frac{da}{dt}$. $I_t \equiv 2\pi \int J_t(r) r dr$ is the toroidal current component. M is the mass of the flux-rope,$M = \pi a^2 \bar{n}_T m_i$. $B_t, B_{pa}, B_p and \beta_p$ are discussed before. In the initial equilibrium state, the total net forces (F_R) acting on the major radius F_R and theat on the minor radius (F_a) are equal to zero, which can be used to infer the initial $B_{pa}, B_s and I_t$ from other parameters.

The toroidal current is also related to the poloidal flux by

$$I_t = \frac{\Phi_p}{cL} \tag{3.10}$$

The inductance function L is described in terms of major radius R, minor radius at footpoint, and minor radius at apex.

$$L(R, a_a, a_f) \equiv \frac{1}{2}[ln\frac{8R}{a_f} + ln\frac{8R}{a_a}] - 2 - \frac{\xi_i}{2} \tag{3.11}$$

The background magnetic field in Chen's model [3] is taken as

$$B_s(Z) = B_{s0}\,\mathrm{sec}\,h^2\frac{(Z_* - Z)}{h1} \quad for \quad Z < Z* \tag{3.12}$$

$$B_s(Z) = B_{s0} \sec h^2 \frac{(Z_* - Z)}{h1} \quad for \quad Z > Z* \tag{3.13}$$

$h1, h2$ are scale lengths of the field. This magnetic field is perpendicular to the toroidal magnetic field B_t of the flux-rope.

Another model is MSOE, which stands for Melon-Seeds-Overpressure-expansion proposed by Siscoe [18]. Melon-Seed means the force acting on the CMEs is not symmetric. So, the CMEs will move in the direction of the greatest force. Overpressure means internal magnetic pressure greater than external magnetic pressure. The MSOE model is to study propagation and expansion for the fast CMEs. In MSOE model, the expansion of CMEs come from the magnetic field inside. The propagation is caused by the magnetic field outside. However, MSOE model does not to consider the internal magnetic structure such as the effect of magnetic tension, which provides a constant force in accelerating CMEs. Therefore, this thesis will largely follow on on Chen's flux rope model, which take into account the internal magnetic field.

In summary, the existing models, serve as the good starting point for me to develop more sophisticated model to fully explain and understand the evolution of CMEs in the interplanetary space observed by STEREO satellite.

Chapter 4: My Previous Work on CMEs and ICMEs

In this section, I summarize the research work I have done in the past three years. The previous work is intimately related with the proposed work. I have worked on identifying CME sources of geomagnetic storms by using data from SOHO/LASCO, SOHO/EIT, ACE and WIND. The work consisted of two parts, the first was to analyze solar sources and the other was to analyze the interplanetary sources. The work was also part of the efforts for the Coordinated Data Analysis Workshop (CDAW) at George Mason in 2005 and at Florida Institute of Technology in 2007. We had studied sources of all major geomagnetic storms from 1996 - 2005, which were defined as the Dst index values less than -100 nT ($Dst \leq -100nT$).

The reasons we selected major geomagnetic storm events using Dst index instead of Kp and Ap index was because that the global ring current casuing the major storms is originated around the earth's equator. Kp and Ap often relate to the sub-storms (and aurora) at high latitudes. We found that the solar and interplanetary sources of these geomagnetic storms can be classified into three types; single type (s-type), multiple types (M-type) and corona hole type (C-type). A single type is caused by a source of CME from the sun and a single ICME. A multiple-typed event is from multiple CMEs from the sun and a complex solar wind flow which is caused by interaction of ICMEs in the interplanetary space corresponding to multiple CMEs from the sun. The C-type is from Corotating Interaction Region or CIR, which occurs from the fast speed stream of solar wind originated from low latitude corona hole; the fast stream catchs up the preceding slow speed stream of solar wind. For a total number of 88 major geomagnetic storms during 1996-2005 is 88, we found that the single type, multiple type and C-type events are 53 (60%), 24 (27%) and 11 (13%) respectively.

4.1 Analyzing Solar Sources

When a geomagnetic storm occurs and the upstream interplanetary solar wind has the signature of an ICME, we need to look at the solar data to identify the solar source. We use the solar data from LASCO/C2, and C3 coronagraphs for identifying CMEs. Extreme Ultraviolet Imaging Telescope or EIT is used to determine the source surface regions of CMEs. CME catalog from NASA and Catholic University is referred in this project. ($http://cdaw.gsfc.nasa.gov/CME\_list/$). Due to the lacking of the observations between the sun and the earth, a search window is used to find sources CME candidates. The search window is 5 days or 120 hours backward from the storm time. Any front-side halo CMEs occurring within the search window are considered as possible sources.

For example, for the geomagnetic storm on April 07, 2000, the search window should be from April 02, 2000. Then the CME catalog was used to find plausible events. The narrow CMEs with angular width less than 120 degree were excluded, because they usually do not direct toward the Earth. According to the CME Catalog, the candidate is on 16:32 UT April 04, 2000. The projected speed of the CME is 1188 km/s and the angular width is 360 degree. Figure 2 shows the snapshot images of the 2000 April 04 event observed by EIT and C2 from SOHO spacecraft.

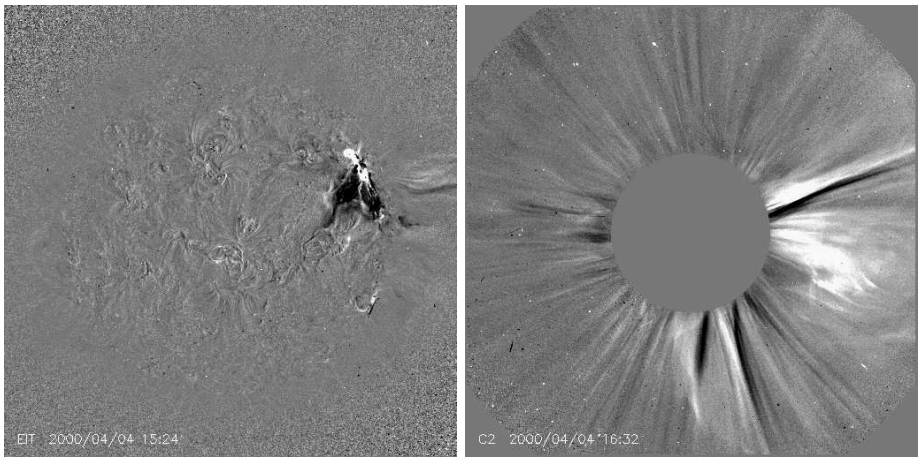

Figure 4.1: The 2000 April 04 CME. The location of the surface source region is indicated by the dimming area in the EIT image(*left*), and the CME itself in LASCO/C2 image(*right*).

The CME was very fast, which required a short time as short as 25 hours to reach the earth. Moreover, the EIT movie showed a clear signature of CME eruption, as indicated by dimming, wave, flare, and an arcade at N16W59. Figure 2 (right) shows the CME coming out from the northwest of the sun, which was consistent with the source surface locations both time and direction. Therefore, this CME was probably the source of the storm.

4.2 Analyzing and Identifying Interplanetary Source

The geo-effective interplanetary structures can be either ICMES or CIRs. Many solar wind signatures can be used to identify ICMEs, which includes low proton temperature ([16]), bidirectional suprathermal electron strahls ([22]), ([8]), enhance plasma helium abundance ([16]), ([2]), enhance Fe charge state ([10]), energetic particles signatures such as bidirectional energetic protons ([15]) and cosmic rays ([6]).

The summary plot (figure 3) displays the solar wind magnetic field and plasma data. It shows the data in time period from April 4, 2000 to April 09, 2000. The first panel contains the Dst plot. Dst is the index used to determine the occurrence of geomagnetic storms. The Dst instruments monitor the earth magnetic field on the ground near mid-latitudes of the earth. The negative value of the Dst index represents how strong the geomagnetic storms are. The more negative the Dst index, the stronger the geomagnetic storm. The Dst index has a negative value because of the diamagnetic process due to the enhancement of the ring current, which flows from east to west. The next panel shows the total magnetic field (black) and the southward component of magnetic field (red) measured in space by ACE instrument. The southward magnetic field is now believed to be the necessary cause of geomagnetic storms. The third panel presents solar wind velocity. The fourth, fifth, sixth, and seventh panels exhibit solar wind density, proton temperature, ratio of observed and expected proton temperature, and plasma beta, respectively. Finally, the last panel plots the solar wind energy input to magnetosphere, which is calculated as

$$\varepsilon = V * B * F(\theta) * L^2 \tag{4.1}$$

The term ε represents the power. When we integrate the power over a certain period of time, we can find the total energy input during this period. The term V is the solar wind velocity. The term B is the magnetic field. The term F (θ) is the function of polar angle of the IMF. Finally, the L term is the linear dimension of the cross section area of the magnetosphere ([1]).

After calculating the magnetosphere energy input for all ICME events, we found an interesting diversified distribution of the drivers of geomagnetic storms. If the energy input from the ICMEs or magnetic cloud is more than 80%, the event is dominantly driven by ICME. For some events, the energy input from shock sheath regions is more than 80%, it means that the storm dominantly driven by the shock sheath. For the event on April 4,2000, the calculation showed that more than 95% of energy input is from the shock sheath region and only 2.1% in the ICME. So, this event is dominantly driven by the shock sheath.

In figure 3, the solar wind interval between the two vertical blue lines (cross all the panel) indicates the period of the presence of the ICME. The signatures of ICMEs are the low plasma beta (< 0.1), high density, low ratio of proton temperature and expectation temperature (≤ 0.5) (also see ([16]). Moreover, as shown by θ angle of the magnetic field, a smooth rotation is evident. The smooth rotation of the southward magnetic field is a strong manifest of a flux rope configuration of the ICME.

Figure 4 shows in detail the magnetic fields. The first plot is the total magnetic field strength. In the region of the ICME, the magnetic field strength is higher than the ambient solar wind. The second, third, and forth panels show the magnetic field component in the x-, y-, and z-directions repectively. The magnetic component of z-direction is important because it co-aligns with the southward magnetic field. The final two panels are the angles, which are used to identify the possible magnetic field rotation.

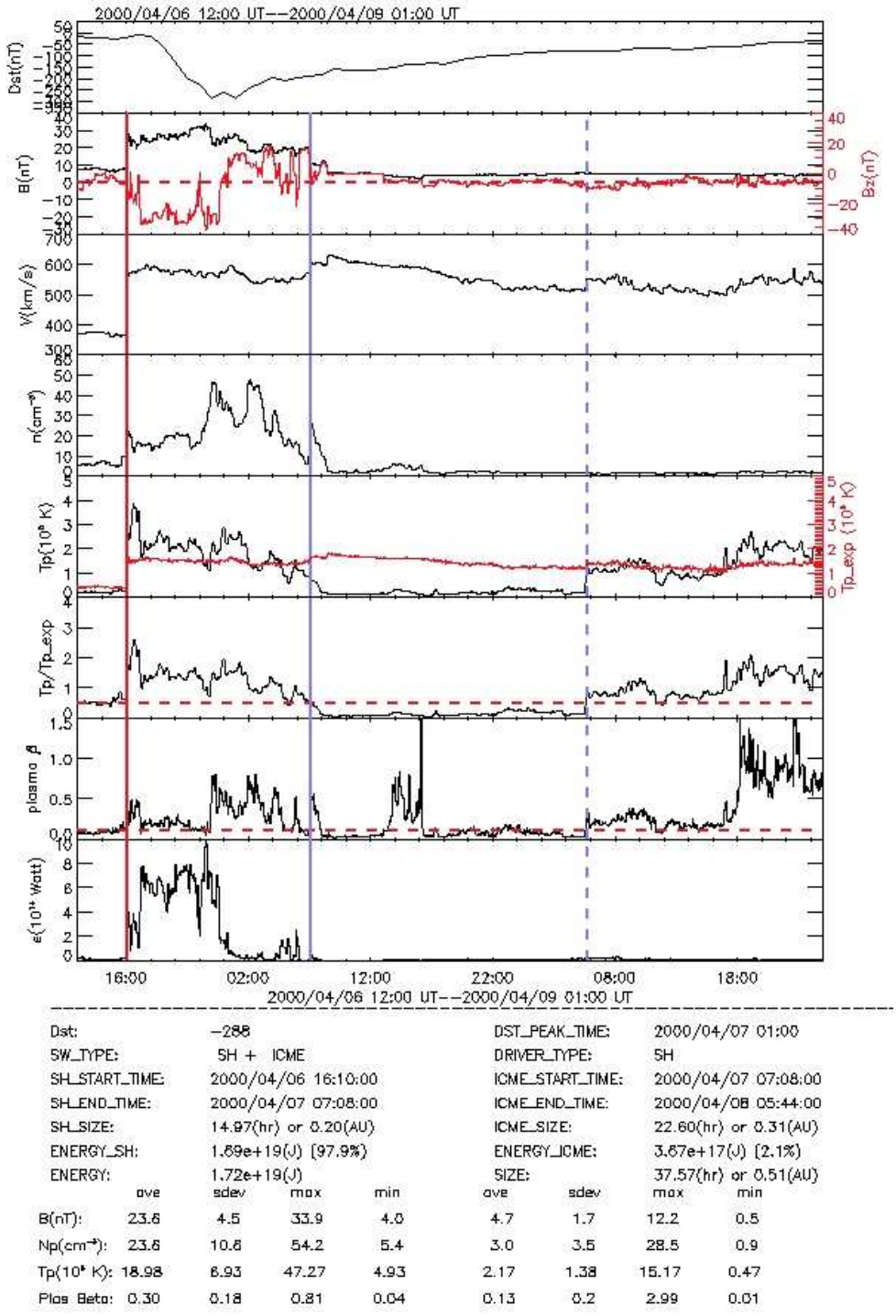

Dst:	−288				DST_PEAK_TIME:	2000/04/07 01:00		
SW_TYPE:	SH + ICME				DRIVER_TYPE:	SH		
SH_START_TIME:	2000/04/06 16:10:00				ICME_START_TIME:	2000/04/07 07:08:00		
SH_END_TIME:	2000/04/07 07:08:00				ICME_END_TIME:	2000/04/08 05:44:00		
SH_SIZE:	14.97(hr) or 0.20(AU)				ICME_SIZE:	22.60(hr) or 0.31(AU)		
ENERGY_SH:	1.69e+19(J) [97.9%]				ENERGY_ICME:	3.67e+17(J) [2.1%]		
ENERGY:	1.72e+19(J)				SIZE:	37.57(hr) or 0.51(AU)		
	ave	sdev	max	min	ave	sdev	max	min
B(nT):	23.6	4.5	33.9	4.0	4.7	1.7	12.2	0.5
Np(cm⁻³):	23.6	10.6	54.2	5.4	3.0	3.5	28.5	0.9
Tp(10⁴ K):	18.98	8.93	47.27	4.93	2.17	1.38	15.17	0.47
Plas Beta:	0.30	0.18	0.81	0.04	0.13	0.2	2.99	0.01

Figure 4.2: Summary plot of solar wind for storm on April 7, 2000

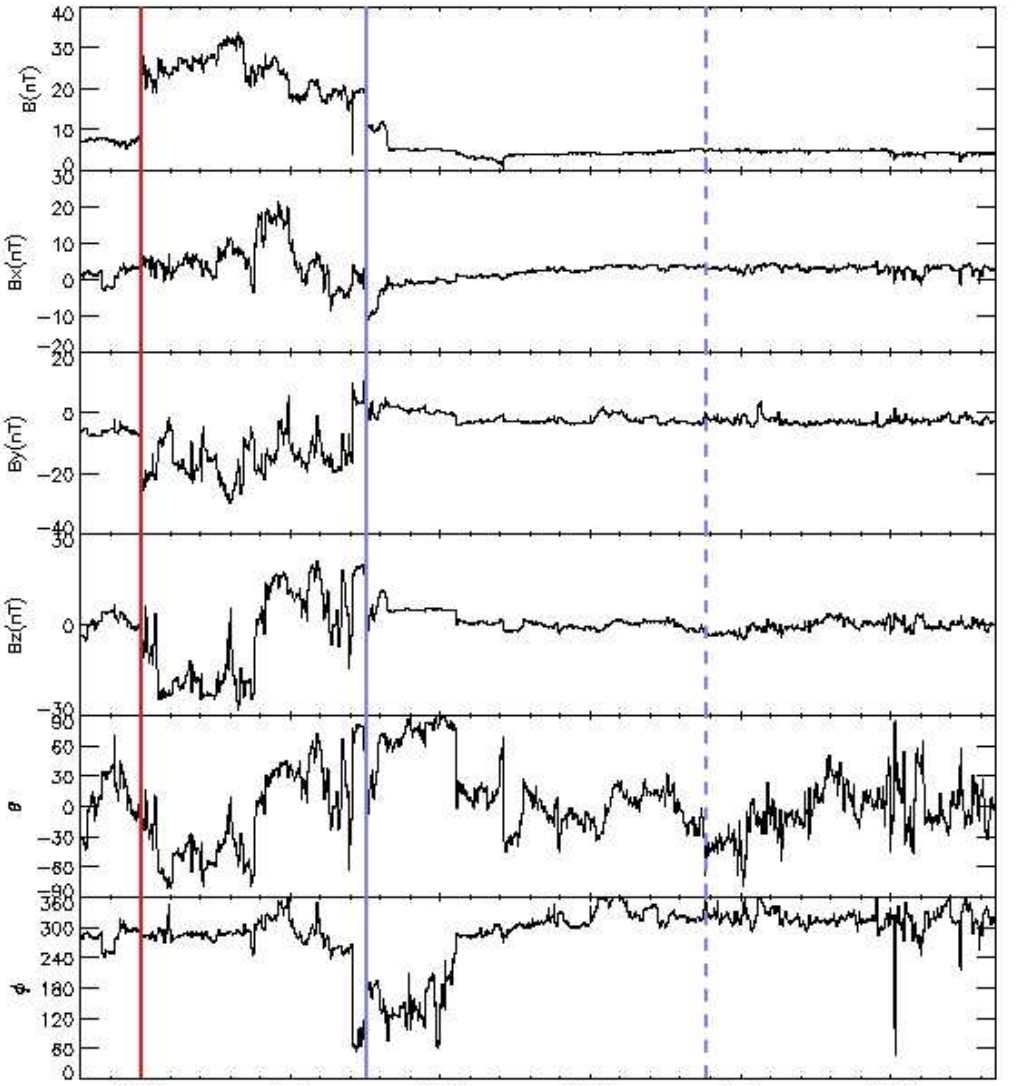

	SH				ICME			
	ave	sdev	max	min	ave	sdev	max	min
B(nT):	23.6	4.5	33.9	4.0	4.7	1.7	12.2	0.5
Bx(nT):	5.1	6.2	21.5	−10.0	1.4	2.7	4.2	−11.0
By(nT):	−14.1	7.6	10.5	−29.6	−1.6	1.9	4.8	−4.1
Bz(nT):	−4.1	15.4	21.0	−28.4	1.3	2.8	11.6	−4.3

Figure 4.3: Magnetic field plot for storm on April 7, 2000

4.3 Publication

- Zhang, J., Richardson, I. F.,Webb, D. F., Gopalswamy, N., Huttinen, E., Kasper, J. C., Nitta, N. V., Poomvises, W., Thompson, B. J., Wu, C.-C, Yashiro, S., and Zhukov, A. N. (2007), Solar and Interplanetary Source of major geomagnetic storms (Dst $< -100nT$) during 1996-2005, *J. Geophys Res.*,112,A10102, doi:10.1029/2007JA01232 [21]

- Zhang, J., Poomvises, W., Richardson, I. F., Size and relative geoeffectiveness of interplanetary coronal mass ejections and the preceding shock sheaths during intense storms in 1996-2005, GRL 112,A10102, doi:10.1029/2007JA01232 [20]

4.4 Presentation

- Poomvises, W., Zhang, J.: Yuming, W.:SPD meetings, Fort Lauderdale, FL [Poster] 2008

- Poomvises, W., Zhang, J.: CDAW meeting in FIT, FL [Invited Talk] 2007

- Poomvises, W., Zhang, J.: Geo-effective Shock Sheaths And ICMEs: Properties And Relations With Solar Sources, SPD meetings, Hawaii [Poster]2007

- Poomvises, W., Zhang, J.: CME, ICME and Major Geomagnetic Storms in Solar Cycle 23rd, SPD meetings, New Hampshire [Poster] 2006

- Poomvises, W., Zhang, J.: Major Geomagnetic Storms and Their Solar Sources in Solar Cycle 23, AGU, Baltimore, [Poster] 2006

- Poomvises, W., Zhang, J.: A study on solar and Interplanetary Drivers of Geomagnetic storms, SHINE, Utah [Poster] 2006

- Poomvises, W., Zhang, J.: SHINE, Hawaii [Poster] 2005

- CDAW meeting in MASON, VA [staff] 2005

Chapter 5: Proposed Observational Work

My dissertation involves both observations and theories. The proposed observational work is discuss in this section and the theoretical part is discussed in the next section.

CME data in my dissertation come mainly from STEREO satellites, the most suitable satellites to studies the kinematical and morphological evolution. The main objectives of STEREO satellites are to understand the causes and mechanisms of CME initiation and the propagation characteristics of CMEs in the interplanetary space. Another objective of STEREO satellites is to study energetic particles, which are accelerated in the low corona and in the interplanetary medium as well.

The instrument on board STEREO consists of Sun Earth Connection Coronal and Heliospheric Investigation (SECCHI),STEREO/WAVES (SWAVES), In-situ Measurements of Particles and CME Transients (IMPACT), PLAsma and SupraThermal Ion Composition (PLASTIC).

Sun Earth Connection Coronal and Heliospheric Investigation (SECCHI) has five instruments, which are an extreme-ultraviolet imager (EUVI), two white-light coronagraphs (COR1 and COR2) and a heliospheric imagers (HI1 and HI2). These instruments study the 3-D evolution of coronal mass ejections from the Sun's surface, through the corona and the interplanetary space, including the Earth.

STEREO/WAVES (SWAVES) is the tracker of an interplanetary radio bursts that measure the evolution of the radio disturbances from the Sun to the orbit of Earth. In-situ Measurements of Particles and CME Transients (IMPACT) provide plasma characteristics of solar energetic particles and the local vector magnetic field. PLAsma and SupraThermal Ion Composition (PLASTIC) provides plasma characteristics of protons, alpha particles, and heavy ions.

5.1 Observations of CMEs

SECCHI/STEREO is suitable for studying CMEs propagation and expansion because it is able to measure CMEs from solar surface (EUVI) to hundreds of solar radius. In my dissertation, I will use the data from COR2, HI 1 and HI 2, which means I will measure CME parameters from 5 solar radius to 1 AU. Moreover, I will use other instruments, ACE, WIND and STEREO/IMPACT, to measure the corresponding ICMEs in-situ. From the SECCHI, images, position and time of CMEs are obtained. When the position and time can be measured in A and B, the 3-D position can be calculated by using triangulation method. Then, 3-D velocity and 3-D acceleration can be calculated by taking first and second derivative of the position and time respectively. The 3-D position, 3-D velocity and 3-D acceleration from SECCHI are free of projection effect components from LASCO/SOHO data.

Figure 5 shows the snapshots images of CME on March 25, 2008. This event occurred on the eastern hemisphere. SECCHI-A detected this event from EUVI to HI 1. Therefore, this CME is one of good events for studying the kinematical and morphological CME evolution from the sun to the interplanetary space.

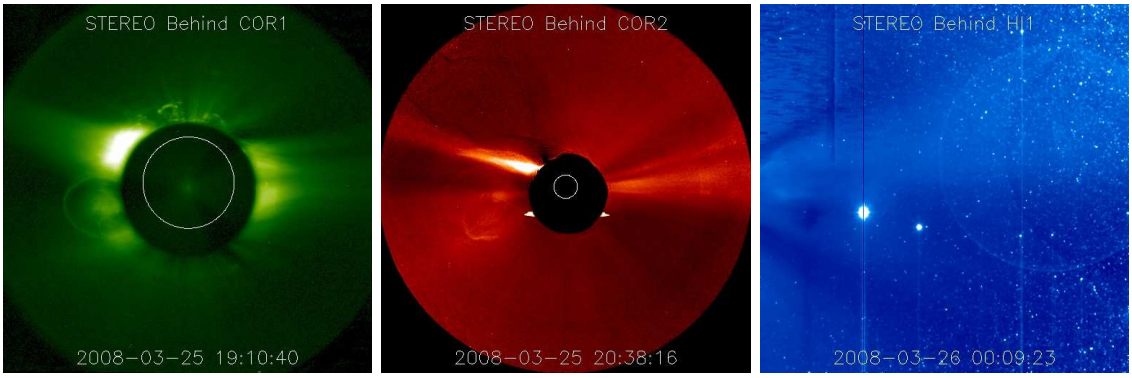

Figure 5.1: Three snapshots of the 2008 March 25 CME taken by COR1 (*left*), COR2 (*middle*) and HI1 (*right*), respectively.

5.2 CME Measurement Using Circular Fitting Method

To measure a CME in 3-D, one model is assumed that the CME is in a spherical shape. Circular fitting method can be applied to STEREO A and B images and calculate the parameters: the centroid of the CME (Z), and radius of the CME (a). The radius means from centroid of the CME to the leading edge of CME. The velocity at the leading edge has two components, the first one is expansion velocity and the second one is the propagation velocity or bulk velocity as measured at the centroid. The expansion velocity can be calculated by taking derivative of $\frac{da}{dt}$, a is the radius of CME. Bulk or propagation velocity can be found from the first derivative of Z, $\frac{dZ}{dt}$, Z is the the height of the CMEs.

The images in figure 5.2 show the circular fitting of the CME on March 25, 2008. Circular fitting is easy to implement and work well in the lower corona from EUVI, COR1 and observations. However, the circular fitting method might not be able to get the accurate measurement from COR2, HI1 and HI 2, because the spherical assumption likely breaks down there. Therefore, I probably apply different methods in the outer corona to better fit the CME geometry. When I tracked CMEs using the multiple instruments, I find another problem. This transition of instruments often make the measurement "jumpy". I need to find appropriate methods to reduce the measurement noise.

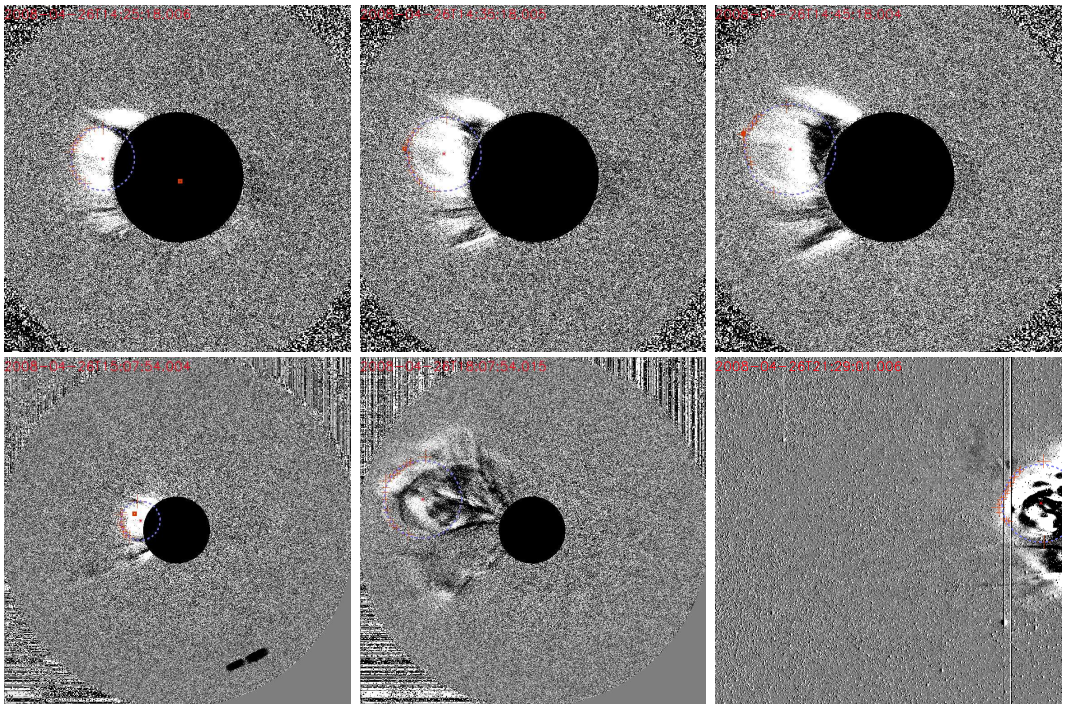

Figure 5.2: Six snapshots of the 2008 April 26 CME taken by COR1, COR2, and HI1, respectively. The first three images in the first row show the circular fitting in COR1, the two images in the second row represent the circular fitting in COR2. The circular fitting in HI 1 shows in the last image of the second row. This event is hard to be seen in HI2 because the CMEs was too faint.

5.3 CMEs Measurement Using Graduated Cylindrical Shell (GCS) Model

In addition to circular fitting method, I will also use the Graduated Cylindrical Shell (GSC) model to measure CME parameters [19] GCS model assumes a flux rope-like structure It is also able to correct for the projection effect. This model can measure the major and minor radius of the flux rope by using STEREO A and B observations. As the project progresses, I will explore other appropriate measurement model to best fit the observations.

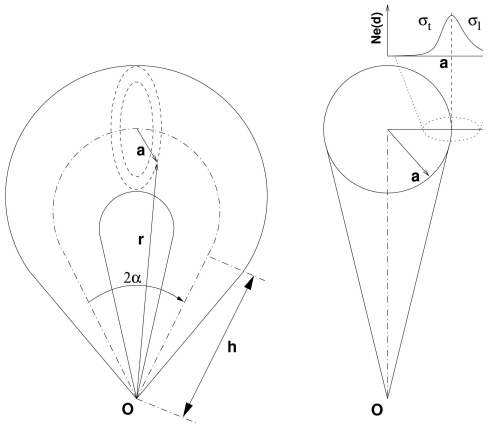

Figure 5.3: Graduated Cylindrical Shell. This figure shows the face-on and edge-on of the flux rope-like model or Graduate Cylindrical Shell model. The dash-dot line shows the axis through the center of model. The solid line represents the plane cut through the cylindrical shell and its origin (adopted from Thernisien et al 2006)

5.4 Events for Study

In my dissertation, I will study at least 4 events, which should be well observed and continuously tracked by COR1, COR2, and HI1 observations. Table 5.1 is the partial list of CMEs observed by SECCHI (Thernisien, private communication, 2008). I will start from this list to select suitable evetns for studying kinetic and morphological evolution of CMEs.

Table 5.1: List of CMEs observed by SECCHI

Evetns list			
Event date	Onset time	Vel	Acc
2007-11-04	2007-11-04 12:00	216.1	9.0
2007-11-16	2007-11-16 09:35	345.1	11.8
2007-12-04	2007-12-04 07:17	265.3	7.0
2007-12-16	2007-12-16 07:51	325.1	4.8
2007-12-31	2007-12-31 00:49	972.0	-5.0
2008-01-02	2008-01-02 10:00	730.8	-6.3
2008-01-23	2008-01-22 23:42	442.3	10.4
2008-01-29	2008-01-28 22:38	245.7	5.0
2008-02-04	2008-02-04 08:23	598.0	7.0
2008-02-12	2008-02-12 06:12	249.2	12.1
2008-02-13	2008-02-12 06:47	224.9	2.9
2008-02-15	2008-02-15 06:19	229.7	8.2
2008-02-23	2008-02-23 19:05	244.0	8.8
2008-03-17	2008-03-17 09:17	221.2	6.9
2008-03-18	2008-03-18 08:08	340.3	8.5
2008-03-25	2008-03-25 18:47	1126.8	-30.6
2008-04-05	2008-04-05 15:49	1042.6	4.0
2008-04-26	2008-04-26 13:53	741.0	1.4
2008-05-17	2008-05-17 10:02	986.5	13.1
2008-05-23	2008-05-23 16:16	331.2	6.1
2008-06-01	2008-06-01 21:44	264.9	5.0
2008-06-12	2008-06-12 05:24	319.1	5.2
2008-06-26	2008-06-26 02:04	389.0	0.9
2008-07-07	2008-07-07 11:29	292.2	15.0

Chapter 6: Proposed Theoretical Work

6.1 Forces Governing CME Evolution

In addition to measure and model-fit the kinematical and morphological parameters of CMEs, the objective of my dissertation in the theoretical aspect is to develop dynamical models to explain the evolution. In the flux rope model, major radial and minor radial equations, which control the bulk propagation motion and expansion motion respectively, are driven by a set of different forces. The major radial equation is controlled by four forces: Lorentz force, thermal pressure force, gravity force and drag force. The net force per unit length in the major radius can be calculated from

$$F_R = \frac{I_t}{C^2 R}[ln(\frac{8R}{a}) + \frac{1}{2}\beta_p - \frac{1}{2}\frac{B_t^2}{B_{pa}^2} + 2\frac{R}{a}\frac{B_s}{B_{pa}} - 1 + \frac{\xi_i}{2}] + F_g + F_d \tag{6.1}$$

The first, fifth, and sixth terms ($ln(\frac{8R}{a} - 1 + \frac{\xi_i}{2})$) are JXB curvature force that push the CME outward. the third term in the equation is the JXB tension force ($-\frac{1}{2}\frac{B_t^2}{B_{pa}^2}$), which always pull the CME down to the surface. Pressure force is $+\frac{1}{2}\beta_p$, which usually pushes CME outward. The forth term is the overlying field Lorentz force, which prevent CME from eruption.

The gravity force might pull the CME down to the surface or push the CME out to the corona because it depends on the relative difference of the density of the flux rope (n_T) that of the solar wind (n_a) with respect to ambient density. If the density of the flux rope is greater than the density of the solar wind, the gravity force will pull the CME down to solar surface. But if the density of ambient solar wind is greater than the density of

flux rope, F_g will pull the flux rope out to the corona, which is equivalent to the buoyancy force. The drag force can also pull or push the CME, because it depends on the velocity difference. If the velocity of the solar wind is greater than the velocity of the flux rope, the F_g will accelerate the flux rope outward. However, if the velocity of ambient is less than the velocity of the flux rope, the flux rope will be decelerated by the drag force.

The minor radial equation, which controls the expansion, can be calculated from

$$F_a = \frac{I_t}{c^2 a}\left(\frac{B_t^2}{B_{pa}^2} - 1 + \beta_p\right) \tag{6.2}$$

As mentioned in section 3, β_p equals to $8\pi(\bar{P} - P_a)/B_{pa}^2$. F_a can be rewritten as $Constant * (B_t^2 - B_{pa} + 8\pi(\bar{P} - P_a))$. So, the net minor radial force depends on the toroidal magnetic field, poloidal magnetic field, pressure of flux rope and ambient pressure. Toroidal magnetic field and pressure of the flux rope tend to expand the minor radius. However, the poloidal magnetic field and the ambient pressure prevent the minor radius from expansion.

In this dissertation, I plan to quantitatively calculate all these forces mentioned above and their variation with distance for a set of CMEs observed by COR1, COR2, and HI1.

6.2 Modeling Flux Rope Parameters

In order to constrain the theoretical models, I need to compare theoretical calculations with observations. In the flux rope model, there are two types of free parameters: flux rope constraint parameters and ambient constraint parameters. Table 6.1-6.3 list their parameters.

Table 6.1 shows the constraint parameters that define the flux rope. All of these parameters can be measured. S_0 and Z_0 can be measured in EUVI. Mass of CMEs can be measured in COR2. These parameters define the initial condition of a flux rope.

Table 6.1: Flux rope constraint parameters

Flux rope constraint parameters		
Parameters	Name	Constraint
S_0	Initial Footpoint separation	EUVI
Z_0	Initial Height of the flux rope	EUVI
M	Initial Mass of the flux rope	Measured in COR2

Table 6.2: Ambient constraint parameters

Ambient constraint parameters / global		
Parameters	Name	Detail
V_0	Ambient solar wind	Prescribed, 0-400 $\frac{Km}{s}$ or
N_a	Ambient density	Prescribed $N_a(Z) = 4 * (3R_s^{-12} + R_s^{-4}) * 10^8 + 3.5 * 10^5 * R_s^2$
T	Ambient temperature	Prescribed $T_a(Z) = T_0 * R_s^{-\alpha}$
B_a	Ambient magnetic field	Prescribed, or PFSS model

Table 6.2 shows the constraint of the ambient parameters: ambient solar wind V_0, ambient solar wind density N_a, ambient temperature T_a and ambient magnetic field B_a. Ambient solar wind usually goes from 0 to 400 $\frac{km}{s}$. The solar wind density and ambient temperature can be prescribed with empirical equations, which I show in Table 6.2.

Table 6.3: Free Parameters Interested in

Free Parameters Interested in		
Parameters	Name	Constraint
C_d	Drag coefficient	Propagation motion
γ	Polytropic index	Expansion motion

Table 6.3 shows the free parameters I am interested in. These parameters can be adjusted to fit the observation. Drag coefficient is in the drag force, which needs to be modified to fit the propagation velocity over a large distance. γ is the polytropic index, which can be found through fitting the expansion equation with observation.

6.3 Dragging Force and Dragging Coefficient

Special attention will be paid toward the dragging force and the dragging coefficient The STEREO provides an unprecedented tracking of CMEs over a large distance, which presents the observational constraints on our understanding of CME dragging. Drag equation in flux rope model comes from the drag force of fluid dynamic, which is

$$F_d = \frac{1}{2} * \rho * u^2 * C_d * A \tag{6.3}$$

ρ is the mass density of the fluid, u is the velocity of the object relative to the fluid,C_d is the drag coefficient, which is dimensionless, A is the reference area. A in the flux rope model is the cross section area per unit length; so, A in the flux rope model is equal to $2a$. The drag force in Chen's paper(1996) is

$$F_d = c_d n_a m_i a \left(V_a - V\right) \mid V_a - V \mid \tag{6.4}$$

Krall et al (2006) [9] mentioned that if V is greater than the ambient solar wind V_c, the flux rope will transfer kinetic energy to the ambient solar wind. Since the effective cross section of the flux rope at apex is equalled to $2 * a$. [4], then the flux rope will be pushing into solar wind with relative velocity $(V + 2V_a - V_c)$, or being pushed by relative velocity $V_c - V + 2V_a$, the drag equation is therefore

$$F_d = \begin{cases} -2C_d n_c m_p a(V + 2V_a - V_c) & V \geq V_c \\ 2C_d n_c m_p a(V_c - V + 2V_a) & V < V_c \end{cases} \tag{6.5}$$

Further, Chen et al(2008) suggested that the drag force need to be modified to

$$F_d = 2 * c_d * a * \rho_a \left(V_{sw} - (V_a - 2w)\right) \mid (V_{sw} - (V_a - 2w) \mid \tag{6.6}$$

V_{sw} represents the solar wind velocity, w is the $\frac{da}{dt}$ is the minor radial expansion speed and ρ_a is the ambient mass density. Moreover, the factor of 2 in this equation come from the minor cross section of CME is taken to have 2 two times larger. Even with these modifications, Chen et al (2008) [5]found that the typical dragging coefficient (order of 1) is not large enough to explain the observations. I need to explore the drag coefficient from the observations.

6.4 Expansion Equation

The expansion equation or minor radial equation needs to be investigated. When I fit the model with observations in a preliminary study, I always find that the expansion velocity from the flux rope model does not match the observation. Chen assumed that the polytropic index of the flux rope model equal to a constant of 1.2. However, according to Wang (2008), he found that the polytropic index decreases with distance. The polytropic index in the flux rope model needs to be investigated. The choice of different index affects the pressure variation of the CME as it expands and decreases density. A different pressure results in difference expansion velocity. Therefore, studying CMEs expansion provides us the opportunity to probe into the state of CMEs plasma, which is otherwise difficult to obtain.

6.5 Methodology for solving Flux rope model

Runge-Kutta algorithm will be used to solve the force equations, which are rewritten as a set of first order ODE's

$$\frac{dZ}{dt} = V \tag{6.7}$$

$$M\frac{dV}{dt} = \frac{I_t^2}{C^2 R}[\ln\frac{8R}{a} + \frac{1}{2}\beta_p - \frac{1}{2}\frac{B_t^2}{B_{pa}^2} + 2\frac{R}{a}\frac{B_s}{B_{pa}} - 1 + \frac{\xi_i}{2}] \tag{6.8}$$

$$+[\pi a^2 m_i g(Z)(n_a - \bar{n}_T)] + [c_d n_a m_i a(V_a - V)|V_a - V|]$$

$$\frac{da}{dt} = w \tag{6.9}$$

$$M\frac{dw}{dt} = \frac{I_t^2}{c^2 R}(\frac{B_t^2}{B_{pa}^2} - 1 + \beta_p) \tag{6.10}$$

where M is the mass of the flux-rope, $M = \pi a^2 \bar{n}^T m_i$.To initialize an eruption, the system must be driven out of equilibrium. Increasing the poloidal flux or equivalently increasing the toroidal current can put the system out of equilibrium. However, I will not focus on initial driven force that make the flux rope loss of equilibrium. Instead I will focus on how a flux rope expand and propagate in the interplanetary space.

Chapter 7: Summary and Timeline

In summary, I propose to study the kinematic and morphological evolution and dynamics of CMEs in the interplanetary space. The data will be obtained from the Solar TErrestrial RElations Observatory (STEREO) satellites. I will develop theoretical models to explain the observations. The first task is to implement and test the existing flux rope models, which solve the propagation and expansion equations using Runke Kutta 4th order method. Then I need to develop the CME fitting model to measure kinematic and morphological parameters of CMEs from STEREO observation. Both circular fitting and GCS fitting methods will be explored. At least 4 events from STEREO satellite will be studied. Then, I need to compare the theoretical models with the observational data from STEREO. Finally, I will develop a successful theoretical model to explain the evolution of CMEs, which consider all the forces involved, including Lorentz force, thermal pressure force, gravity force and solar wind dragging force.

The following is a preliminary timeline;

Table 7.1: Ambient constraint parameters

Ambient constraint parameters	
Time Period	Detail
$September - November$	Testing and Solving flux rope model
$December - January$	Observation from SECCHI/STEREO + Circular fitting
$February - March$	Observation from IMPACT/STEREO + GCS (if needed)
$April - July$	Developing the theoretical model
$August - September$	Testing new theoretical model with STEREO data set

Bibliography

Bibliography

[1] S. I. Akasofu. Energy coupling between solar wind and magnetosphere. *Space Science Reviews*, 28:121–190, 1981.

[2] G. Borrini, J. T. Gosling, S. J. Bame, and W. C. Feldman. Helium abundance enhancements in the solar wind. *J. Geophys Res*, 87:7370–7378, 1982.

[3] J. Chen. Effects of toroidal forces in current loops embedded in a background plasma. *Astrophys. J.*, 338:453–470, 1989.

[4] J. Chen and Jonathan Krall. Acceleration of coronal mass ejections. *Journal of Geophy Res.*, 108, 2003.

[5] J. Chen and V. Kunkel. Temporal and physical relationships between cme acceleration and flare energy release. *Amer Geophys Union*, Fall Meeting 2008, 2008.

[6] V. M. Dvornikov, I. G. Richardson, V. E. Sdobnov, and H. V. Cane. Bidirectional particle flows at cosmic ray and lower (1 mev) energies and their association with interplanetary coronal mass ejections/ejecta. *Journal of Geophysical Research*, 105:12579–12592, 2000.

[7] N. Gopalswamy, A. Lara, R. P. Lepping, M. L. Kaiser, D. Berdichevsky, and O. C. St. Cyr. Interplanetary acceleration of coronal mass ejections. *Geophys. Res. Lett*, 27:145–148, 2000.

[8] J. T. Gosling, M. F. Thomsen, S. J. Bame, and R. D. Zwickl. The eastward deflection of fast coronal mass ejecta in interplanetary space. *Sol Phys*, 92:12399–12406, 1987.

[9] J. Krall and O. C. St. Cyr. Flux-rope coronal mass ejection geometry and its relation to observed morphology. *Astrophys. J.*, 652:1740–1746., 2006.

[10] S. T. Lepri, T. H. Zurbuchen, L. A. Fisk, I. G. Richardson, H.V. Cane, and G. Gloeckler. Iron charge distribution as an identifier of interplanetary coronal mass ejections. *J. Geophys. Res.*, 106:231–238, 2001.

[11] Y. Liu, J.D. Richardson, and J.W. Belcher. A statistical study of the properties of interplanetary coronal mass ejections from 0.3 to 5.4 au. *Planetary and Space Science*, 53:3–17, 2005.

[12] R. E. Lopez, J. W. Freeman, and E. C. Roelof. The relationship between proton temperature and momentum flux density in the solar wind. *Sol Phys*, 13:640–643, 1986.

[13] M. J. Owen, and Siscoe G. Crooker, N. U., C. Pagle, and P. J. Cargill. Characteristic magnetic field and speed properties of interplanetary coronal mass ejections and their sheath regions. *J. Geophys Res.*, 110A1, 2005.

[14] M. J. Reiner, M. l. Kaiser, and J. L. Bougeret. Solar wind ten. *Amer. Ins. Phys.*, 679:152–155, 2003.

[15] I. G. Richardson and D. V. Reames. Bidirectional 1 mev ion intervals in 1973-1991. *Astrophys. J. Suppl. Ser.*, 85, 1993.

[16] I. G. Richardson and Cane H. V. Regions of abnormally low proton temperature in the solar wind (1965-1991) and their association with ejecta. *J. Geophys. Res.*, 100:397–23, 1995.

[17] I. G. Richardson and H. V. Interplanetary coronal mass ejections in the near-earth solar wind during 1996-2002. *J. Geophys. Res.*, 108, 2003.

[18] G. L. Siscoe, N. U. Crooker, and H. A. Elliott. Initial-condition influences on cme expansion and propagation. *Springer*, 239:293–316, 2006.

[19] A. Thernisien, R. A. Howard, and A. Vourlidas. Modeling of flux rope coronal mass ejections. *Astrophys. J.*, 652:763–773, 2006.

[20] J. Zhang, W. Poomvises, and I. F. Richardson. Size and relative geoeffectiveness of interplanetary coronal mass ejections and the preceding shock sheaths during intense storms in 1996-2005. *J. Geophys Res*, 112, 2007.

[21] J. Zhang, I. F. Richardson, D. F. Webb, N. Gopalswamy, E. Huttinen, J. C. Kasper, N. V. Nitta, W. Poomvises, B. J. Thompson, and Yashiro S. and Zhukov A. N. Wu, C.-C. Solar and interplanetary source of major geomagnetic storms (dst $< -100nt$) during 1996-2005. *J. Geophys Res.*, 112:A10102, 2007.

[22] R. D. Zwickl, J. R. Asbridge, S. J. Bame, W. C. Feldman, J. T. Gosling, and E. J. Smith. Plasma properties of driver gas following interplanetary shocks observed by isee-3. *Solar Wind Five*, 2280:711, 1983.